Immersion freezing of surface dust particles from Tengger Desert in China: effects of mineral composition and aging treatments on ice nucleating activity

Jiao Xue[1], Shengkai Wang[1], Haoyu Qi[1], Yao Yao[1], Shulan Chen[1], Juying Lu[1], Tian Zhang[1], Qi Wang[2], Defeng Zhao[3], Youwei Hong[4], Yihua Cai[1], Bingbing Wang[1,*]

[1]State Key Laboratory of Marine Environmental Science, College of Ocean and Earth Sciences, Xiamen University, Xiamen, China

[2]China-ASEAN College of Marine Sciences, Xiamen University Malaysia, Selangor Darul Ehsan, Malaysia

[3]Shanghai Key Laboratory of Ocean-land-atmosphere Boundary Dynamics and Climate Change, Fudan University, Shanghai, China

[4]School of Resource and Environmental Science, Quanzhou Normal University, Quanzhou, China

* *Corresponding authors:* Bingbing Wang (Bingbing.Wang@xmu.edu.cn)

Table S1. Sample information for ice nucleation parameterization of compositional complex dust in Fig. 5(c) from previous studies.

Reference of parameterization	Sample description
Hader et al., 2014	Commercial ATD
Niemand et al., 2012	(1) Soil sample collected in the eastern parts of the Takla Makan Desert in China
	(2) Soil sample collected about 50 km north of Cairo, Egypt
	(3) Soil sample collected near the town of Mala on the Canary Island of Lanzarote
	(4) Sedimented particles after a dust storm in Israel
	(5) Milled reference dust material, Powder Technology, Inc., Minnesota
Ullrich et al., 2017	(1) Asian desert dust Collected from the ground in the eastern parts of the Takla Makan desert in China, east of the Dalimu basin between Kuerle and Ruoquiang
	(2) Canary Island dust collected from the ground near Mala, Lanzarote, Canary Islands
	(3) Israel desert dust collected as sediment particles after a Saharan dust storm event in Tel Aviv, Israel
	(4) Saharan desert dust collected from a hole of 1.5-m depth about 70 km northeast of Cairo, Egypt
	(5) Saharan desert dust collected 50 km north of Cairo, Egypt as sediment particle after sand storm event
	(6) Saharan desert dust collected in Morocco
	(7) Saharan desert dust collected as soil sample in southern Tunisia near Tozeur
Reicher et al., 2019	Airborne aerosol in dust events collected in Rehovot, Israel
Chen et al, 2021	Airborne aerosol in dust events collected in Beijing, China

Table S2 The *m* and *n* values for the parameterizations of N_s as a function of *T*, J_{het} as a function of Δa_w, and J_{het} as a function of *T*.

Parameterization	**Samples**	m	LCL_m	UCL_m	n	LCL_n	UCL_n	$RMSE$	R^2
$\log(N_s) = m_1 \times T + n_1$	Us-dust	-0.46	-0.49	-0.43	123.93	117.00	130.85	0.30	0.95
	S-dust	-0.41	-0.45	-0.37	110.94	100.68	121.19	0.31	0.91
	Us-dust (0.0187. wt%)	-0.43	-0.46	-0.39	114.81	106.73	122.88	0.10	0.99
	Add 5×10^{-5} M AS	-0.45	-0.48	-0.43	122.15	115.00	129.30	0.10	0.99
	Add 5×10^{-4} M AS	-0.32	-0.36	-0.29	89.15	79.97	98.33	0.16	0.97
	Add 1×10^{-3} M AS	-0.54	-0.60	-0.47	145.00	128.45	161.56	0.15	0.98
	Add 2×10^{-3} M AS	-0.40	-0.44	-0.36	109.98	100.59	119.37	0.08	0.99
	Add 5×10^{-3} M AS	-0.45	-0.48	-0.41	121.96	111.84	132.09	0.12	0.98
	Add 5×10^{-2} M AS	-0.39	-0.40	-0.37	106.23	102.25	110.21	0.05	1.00
	Add 5×10^{-4} M NaCl	-0.36	-0.40	-0.32	98.72	88.26	109.18	0.14	0.97
	Add 5×10^{-3} M NaCl	-0.46	-0.51	-0.41	123.54	111.48	135.59	0.14	0.98
	Add 5×10^{-2} M NaCl	-0.52	-0.58	-0.46	139.24	123.91	154.57	0.17	0.97
	Add 2.5×10^{-4} M H_2SO_4	-0.62	-0.68	-0.56	164.88	149.20	180.56	0.13	0.99
	Add 2.5×10^{-3} M H_2SO_4	-0.58	-0.67	-0.50	155.15	132.95	177.36	0.17	0.97
	Add 2.5×10^{-2} M H_2SO_4	-0.49	-0.58	-0.41	131.80	110.46	153.14	0.22	0.95
	Add 5×10^{-3} M HNO_3	-0.33	-0.37	-0.29	89.77	79.95	99.60	0.19	0.96
	Add 5×10^{-3} M HNO_3	-0.32	-0.36	-0.28	87.67	77.50	97.85	0.18	0.96
	Add 5×10^{-2} M HNO_3	-0.49	-0.53	-0.45	131.03	120.00	142.06	0.10	0.99
	Heating treatment	-0.59	-0.64	-0.54	156.02	142.61	169.43	0.12	0.99
$\log(J_{het}) = m_2 \times \Delta a_w + n_2$	Us-dust	54.57	51.07	58.07	-7.21	-7.78	-6.64	0.34	0.94
	S-dust	42.72	37.80	47.65	-6.19	-7.11	-5.27	0.33	0.87
	Us-dust (0.0187 wt%)	44.36	37.54	51.18	-5.97	-7.05	-4.89	0.19	0.94
	Add 5×10^{-5} M AS	49.88	43.12	56.64	-6.60	-7.60	-5.59	0.21	0.95
	Add 5×10^{-4} M AS	37.29	29.98	44.61	-4.16	-5.13	-3.20	0.29	0.90
	Add 1×10^{-3} M AS	50.87	43.36	58.38	-5.77	-6.77	-4.76	0.16	0.96
	Add 2×10^{-3} M AS	37.82	32.12	43.52	-3.62	-4.36	-2.88	0.12	0.96
	Add 5×10^{-3} M AS	42.57	38.96	46.19	-3.89	-4.32	-3.47	0.10	0.98
	Add 5×10^{-2} M AS	42.46	37.84	47.08	-3.99	-4.53	-3.46	0.14	0.97
$\log(J_{het}) = m_3 \times T + n_3$	Us-dust	-0.45	-0.48	-0.42	116.54	109.41	123.66	0.33	0.94
	S-dust	-0.34	-0.38	-0.30	87.27	77.32	97.22	0.34	0.87
	Us-dust (0.0187wt%)	-0.37	-0.42	-0.31	94.35	79.92	108.77	0.19	0.94
	Add 5×10^{-5} M AS	-0.42	-0.47	-0.36	107.51	93.39	121.63	0.20	0.95
	Add 5×10^{-4} M AS	-0.32	-0.38	-0.26	83.05	67.26	98.84	0.29	0.90
	Add 1×10^{-3} M AS	-0.43	-0.50	-0.37	112.31	95.52	129.09	0.16	0.96
	Add 2×10^{-3} M AS	-0.32	-0.37	-0.27	84.78	72.30	97.26	0.12	0.96
	Add 5×10^{-3} M AS	-0.37	-0.40	-0.34	96.98	88.60	105.35	0.11	0.98
	Add 5×10^{-2} M AS	-0.32	-0.36	-0.27	84.15	72.57	95.72	0.15	0.95

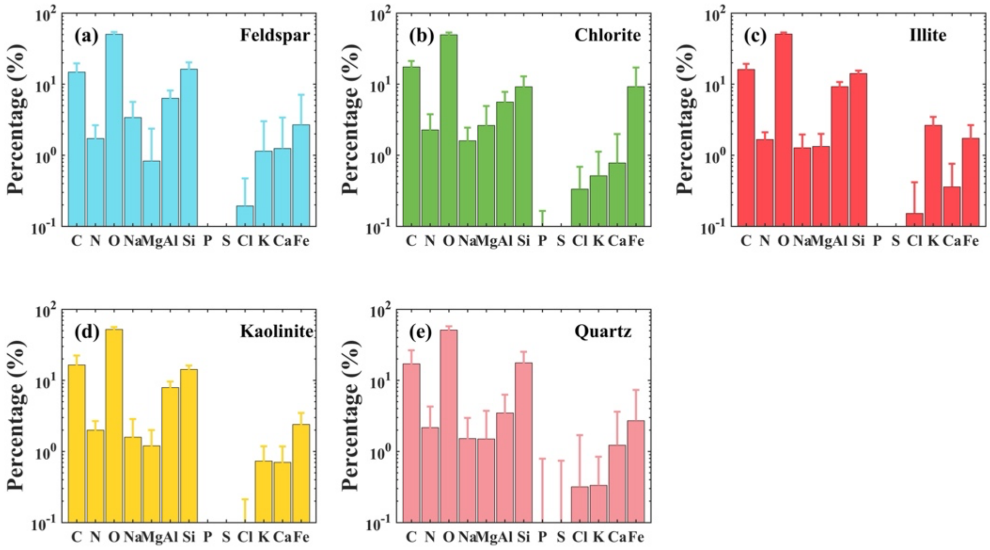

Figure S1. Mean atomic percentages of elements for each dust type from CCSEM/EDX analysis. Overall, all particles exhibit high abundances of O, Si, and Al, reflecting the typical elemental characteristics of silicate minerals. In addition to Si and Al, Feldspar contains non-negligible proportions of Na, K, and Ca. Chlorite is characterized by notably higher proportions of Fe and Mg, whereas illite exhibits a prominent K peak. For Kaolinite, apart from the major elements (O, Si, and Al), the abundances of other metallic elements (e.g., Fe, K, Ca, and Mg) are relatively low. Quartz is dominated by Si and O, with a relatively low Al content lower than Si.

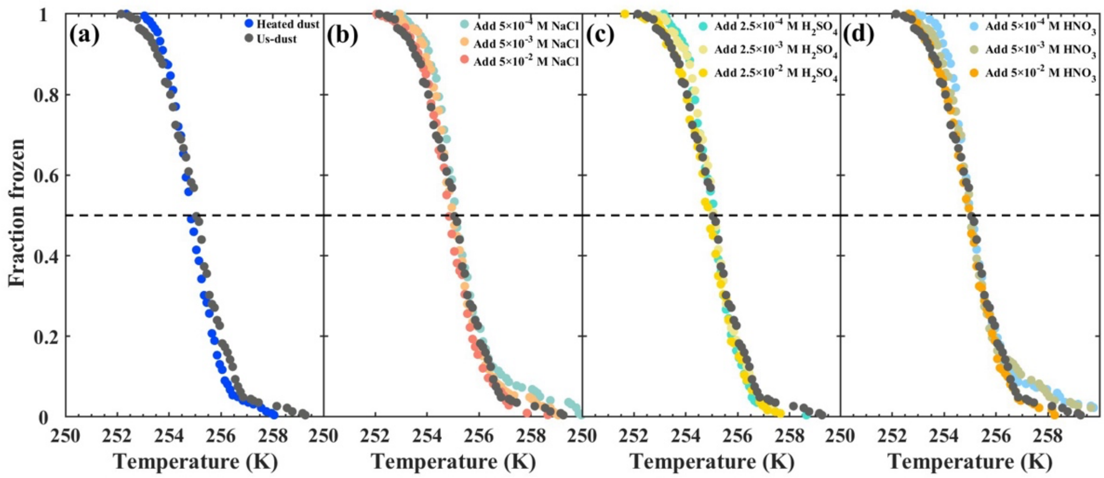

Figure S2. Frozen fraction for droplets with Us-dust (gray dots) and U-dust treated by heating (a) and added to NaCl (b), H_2SO_4 (c), and HNO_3 (d) (dots with different colors).

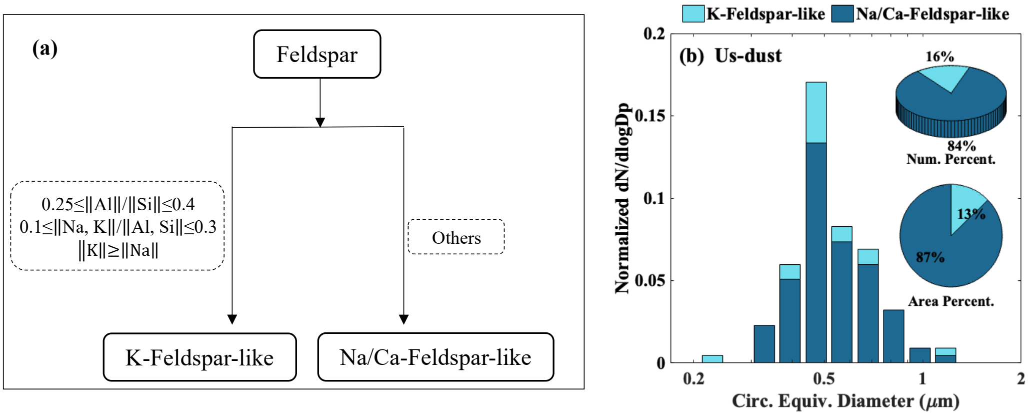

Figure S3. Separation of feldspar in Us-dust into K-feldspar and Na/Ca-feldspar. (a) Classification scheme; (b) Classification results, including normalized particle size distribution, number percentage and surface area percentage of K-feldspar and Na/Ca-feldspar in feldspar particles.

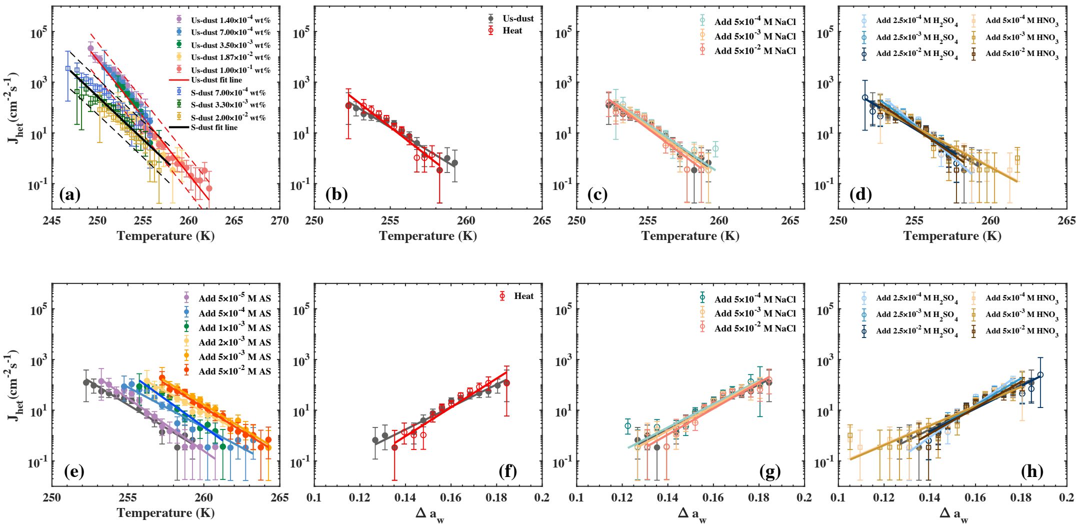

Figure S4. Heterogeneous ice nucleation rate coefficient (J_{het}) as a function temperature (a, b, c, d, e) and a_w (e, f, g) for Us-dust, S-dust, and Us-Dust (1.87×10^{-2} wt%) treated by heating and added to NaCl, H_2SO_4 HNO_3, and AS solution. The gray lines (b-g) are fits lines to the Us-Dust (1.87×10^{-2} wt%). Solid fitting lines (a, e) are parameterizations according to $\log(J_{het}) = m \times T + n$, and the values of m and n parameters are listed in Table S2.

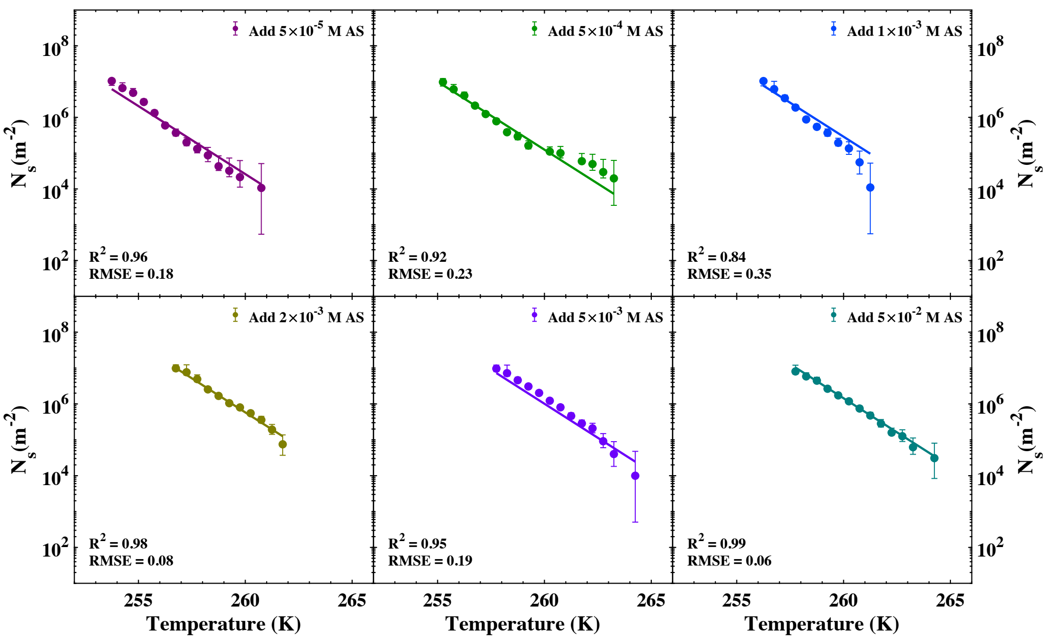

Figure S5. Comparison of the parameterized N_s (T, r) with experimental data. Solid lines represent the parameterizations of N_s (T, r) according to with Eq.9. Colored dots represent the experimental data.

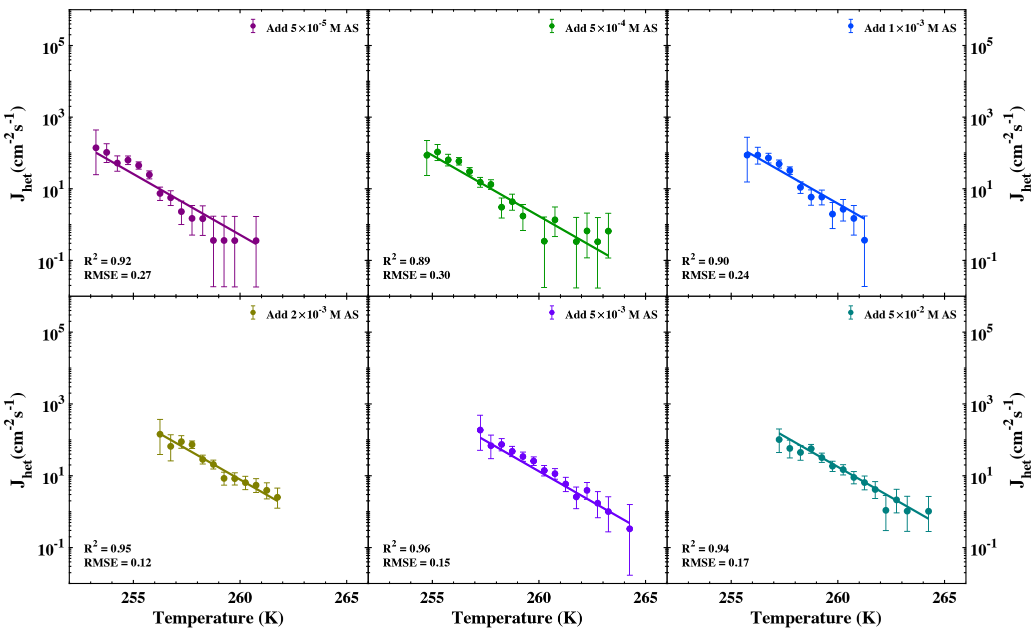

Figure S6. Comparison of the parameterized J_{het} (T, r) with experimental data. Solid lines represent the parameterizations of J_{het} (T, r) according to with Eq.10. Colored dots represent the experimental data.

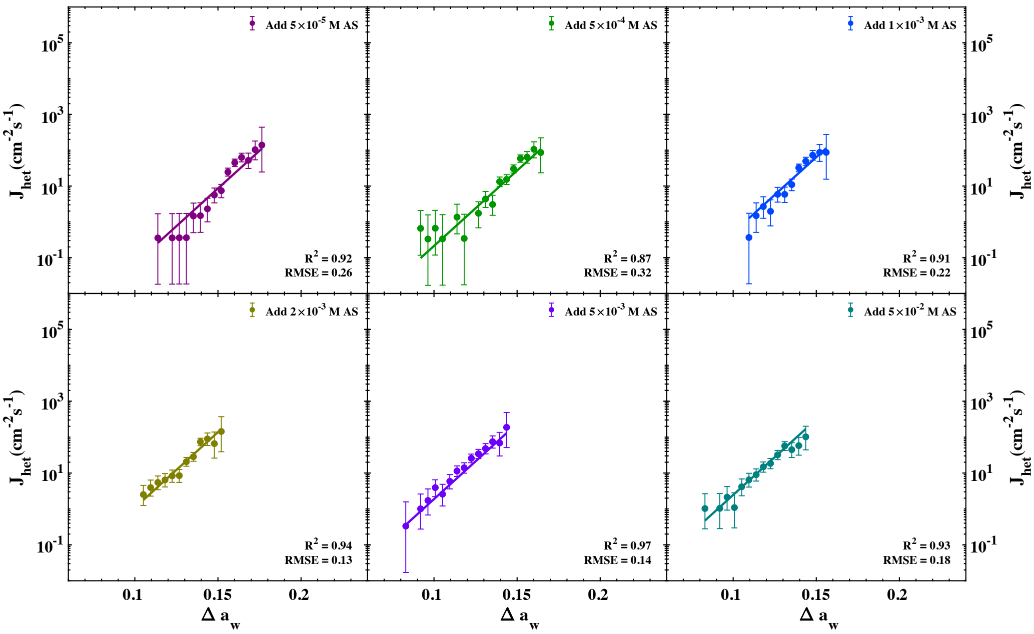

Figure S7. Comparison of the parameterized J_{het} (Δa_{w}, r) with experimental data. Solid lines represent the parameterizations of J_{het} (Δa_{w}, r) according to Eq.11. Colored dots represent the experimental data.